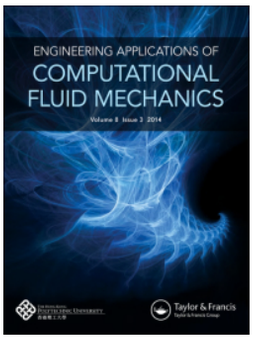

Taylor & Francis
Taylor & Francis Group

Engineering Applications of Computational Fluid Mechanics

ISSN: (Print) (Online) Journal homepage: https://www.tandfonline.com/loi/tcfm20

Efficacy of applying discontinuous boundary condition on the heat transfer and entropy generation through a slip microchannel equipped with nanofluid

Suhong Liu, Dariush Bahrami, Rasool Kalbasi, Mehdi Jahangiri, Ye Lu, Xuelan Yang, Shahab S. Band, Kwok-Wing Chau & Amir Mosavi

To cite this article: Suhong Liu, Dariush Bahrami, Rasool Kalbasi, Mehdi Jahangiri, Ye Lu, Xuelan Yang, Shahab S. Band, Kwok-Wing Chau & Amir Mosavi (2022) Efficacy of applying discontinuous boundary condition on the heat transfer and entropy generation through a slip microchannel equipped with nanofluid, Engineering Applications of Computational Fluid Mechanics, 16:1, 952-964, DOI: 10.1080/19942060.2022.2057591

To link to this article: https://doi.org/10.1080/19942060.2022.2057591

Published online: 01 Apr 2022.

ENGINEERING APPLICATIONS OF COMPUTATIONAL FLUID MECHANICS
2022, VOL. 16, NO. 1, 952–964
https://doi.org/10.1080/19942060.2022.2057591

Efficacy of applying discontinuous boundary condition on the heat transfer and entropy generation through a slip microchannel equipped with nanofluid

Suhong Liu[a], Dariush Bahrami [b], Rasool Kalbasi[c], Mehdi Jahangiri[d], Ye Lu[e], Xuelan Yang[f], Shahab S. Band[g], Kwok-Wing Chau [h] and Amir Mosavi [i,j,k]

[a]School of Mathematics and Information Science, Baoji University of Arts and Sciences, Baoji, People's Republic of China; [b]Department of Mechanical Engineering, Shahrekord University, Shahrekord, Iran; [c]Department of Mechanical Engineering, Najafabad Branch, Islamic Azad University, Najafabad, Iran; [d]Department of Mechanical Engineering, Shahrekord Branch, Islamic Azad University, Shahrekord, Iran; [e]School of Computer Science, Baoji University of Arts and Sciences, Baoji, People's Republic of China; [f]School of Computer Sciences, Universiti Sains Malaysia, Penang, Malaysia; [g]Future Technology Research Center, College of Future, National Yunlin University of Science and Technology, Douliou, Taiwan; [h]Department of Civil and Environmental Engineering, Hong Kong Polytechnic University, Hong Kong, People's Republic of China; [i]John von Neumann Faculty of Informatics, Obuda University, Budapest, Hungary; [j]Institute of Information Engineering, Automation and Mathematics, Slovak University of Technology in Bratislava, Bratislava, Slovakia; [k]Institute of The Information Society, University of Public Service, Budapest, Hungary

ABSTRACT

In this study, the laminar nanofluid flow in the microchannel with a discontinuous-boundary condition was investigated. Considering the slip condition, heat transfer and entropy generation were studied. Different layouts with the discontinuous-boundary condition (i.e. layouts A, B and C) were introduced and compared with the basic microchannel (microchannel with the continuous-boundary condition). Reynolds number and non-slip coefficient parameters on the effect of using discontinuous-boundary condition were discussed. The results revealed that the application of discontinuous-boundary condition affects the heat transfer as well as entropy generation so that the effects are more pronounced at higher Reynold number. By applying discontinuous-boundary condition, the heat transfer through the layouts of A, B and C was 34, 45 and 53% higher than the base microchannel. Simultaneously, the entropy generation through the layouts of A, B and C intensified by 31, 39 and 46%, respectively. The results proved that the applying slip condition has two positive effects as well as a negative effect. It enhanced the heat transfer and diminished the viscose entropy generation, but on the other hand, it intensified the thermal entropy generation.

ARTICLE HISTORY
Received 8 September 2020
Accepted 14 March 2022

KEYWORDS
Microchannel; discontiniuos-boundary condition; slip velocity; entropy generation; heat transfer

1. Introduction

The investigations on the micro-scale devices (Xu et al., 2022) is fundamental in many industries such as aerospace (Weiß et al., 2019), electronics systems (Abo-Zahhad et al., 2019; Ma et al., 2019; Vajdi et al., 2020), photovoltaic–thermal systems (Ahmed & Radwan, 2017; Radwan et al., 2016), concentrator solar cells (Abo-Zahhad et al., 2020), etc. For the enhancement of the heat transfer on the micro-scale the microchannels are essential. Microchannels have a wide range of applications from microfluidics devices (Lai & Wong, 2021) to electronic devices for the quality of a better heat exchange. There are various methods to enhance the heat transfer including active methods such as magnetohydrodynamic (Jarray et al., 2020; Mehrez et al., 2015) and passive methods like adding nanoparticles to the base fluid (Li et al., 2021; Mehrez & El Cafsi, 2017, 2021a, 2021b; Sun et al., 2021). However, most methods result in a considerable pressure loss. Applying discontinuous-boundary conditions has been widely used in heat transfer cases (Bahrami et al., 2019; Ma et al., 2019; M. Mansour et al., 2018; Toghraie et al., 2019). Microchannels have a high surface-to-volume ratio and can be valuable in the cooling issue. The knowledge of material science has a vital role in industries(Kuskov et al., 2021; Torosyan et al., 2020) and shows by improving the thermal properties of the working fluid, the microchannels thermal performance can be enhanced (Huminic & Huminic, 2020). The thermal conductivity of nanoparticles is very high and many researchers have proven that adding nanoparticles to base fluids improves the thermal conductivity (Zahmatkesh et al., 2021).

By examining the second law of thermodynamic systems, the degree of deviation from the ideal state will

CONTACT Shahab S. Band shamshirbands@yuntech.edu.tw; Amir Mosavi amir.mosavi@kvk.uni-obuda.hu

be determined. The second law is examined from two perspectives of entropy (Chamkha et al., 2017; Mansour et al., 2019; Mehrez et al., 2015; Rashad et al., 2018; Rashad et al., 2019; Zamzari et al., 2015) or exergy balance equations (Tian et al., 2020). The entropy generation ($\dot{S}_{gen}$) is concerned with the entropy balance equation (Mansour et al., 2019; Rashad et al., 2018; Rashad et al., 2019) while the exergy loss is obtained through solving the exergy balance equation (Abo-Zahhad et al., 2019; Abo-Zahhad et al., 2020) . Huminic and Huminic (2020) presented a valuable study on the entropy-based second law analysis in which the viscous entropy generation ($\dot{S}_f$) as well as thermal entropy generation ($\dot{S}_t$), are discussed comprehensively. Many studies have identified the effect of nanofluids on entropy production (Ishak et al., 2019; Shashikumar et al., 2018; Tayebi & Chamkha, 2019). Singh et al. (2010) theoretically studied the entropy generation through the microchannel in the presence of $Al_2O_3 - water$ nanofluid (one of the first work in this field). The flow regime was considered laminar and turbulent. They established the correlations by which the ratio of entropy generation in the presence of nanofluids to the entropy generation in the presence of base fluid ($\dot{S}^{nf}_{gen}/\dot{S}^{bf}_{gen}$) can be determined. They proved that under the turbulent flow, incorporation of Al_2O_3 into water diminished $\dot{S}_{gen}$. Ebrahimi et al. (2016) investigated $\dot{S}_{gen}$ through a rectangular cavity (with a 20 kW boundary condition at the left surface) to determine the effect of the presence of Al_2O_3 and CuO nanoparticles. The results showed that the presence of both nanofluids reduced $\dot{S}_{gen}$. However, the decremental effect of adding CuO on $\dot{S}_{gen}$ is greater than the decremental effect of the incorporation of Al_2O_3 nanoparticles. In another study conducted by Heshmatian and Bahiraei (2017), the effects of the presence of TiO_2 nanoparticles in water have been investigated. The authors focused on the particle migration to determine $\dot{S}_f$ and $\dot{S}_t$ considering the Brownian diffusion using ANN. They found that as the nanoparticles size decreased, $\dot{S}_{gen}$ intensified. By solving the energy and momentum equations, Yang et al. (2015) determined the temperature as well as the velocity inside a trapezoidal cavity (nanofluid impregnated). They calculated the thermal and $\dot{S}_f$ considering the temperature gradients as well as the velocity gradients and found that $\dot{S}_t$ contribution to the viscous entropy production was about three times. Also, they observed that the zones with large $\dot{S}_t$ was located at the bottom side of the cavity. According to the results, as the Reynolds number (Re) decreased, $\dot{S}_f$ diminished while $\dot{S}_t$ amplified. The second law of analysis of a counter flow micro-heat exchanger was examined by Mohammadian et al. (2014). The hot fluid (water) flows into the inner tube and the cold fluid ($Al_2O_3/water$) flows through the annular space. It was found that with increase in nanoparticle size and decrease in volume fraction, $\dot{S}_f$ diminished. In contrast, the thermal entropy generation intensified. As the thermal entropy generation contribution has a higher value than the viscous one, so $\dot{S}_{gen}$ intensified with increase in particle size and decrease in volume fraction. The effect of hybrid nanofluid presence with non-Newtonian behavior on the thermal performance of a microchannel heat sink was investigated by Al-Rashed et al. (2019). They examined the effects of adding CNT/Fe_3O_4 to the water on $\dot{S}_{gen}$. The simulation results revealed that by rising Re to the critical number ($Re = 300$), $\dot{S}_{gen}$ diminished. As Re increases upon the critical value, $\dot{S}_{gen}$ will rise. In the meantime, the use of numerical methods has been widely considered.

In this study, the laminar nanofluid flow in the microchannel with a discontinuous boundary condition was investigated. The major aim of this study is to boost the heat transfer without increasing pressure loss in the microchannel. To this goal, this study answers the question of whether heat transfer can be improved by applying discontinuous-boundary conditions? For this, we introduced three layouts to examine the effects of discontinuous-boundary conditions on heat transfer. Then, by examining the second law, the question is answered: what effect does the application of discontinuous-boundary conditions have on the entropy generation? It seems that owing to the presence of an adiabatic zone between the hot zones, the temperature gradients in hot zones intensify and therefore the heat transfer increases. The question then is answered that whether the heat transfer improvement made by applying discontinuous-boundary conditions is accompanied by more entropy generation or less?

2. Problem description

In this study, as shown in Figure 1, the microchannel walls were divided into two equal parts, with 25% of the walls subjected at constant temperature and the remaining 75% is adiabatic. The ratio of length to the height of the microchannel was considered 40. The main purpose of this study is to examine the hot-walls arrangement on HT as well as $\dot{S}_{gen}$. Figure 1 illustrates the different arrangements of the hot walls. Given the slip conditions, the Al_2O_3-water nanofluid enters the microchannel at a temperature of $T_c = 300K$. The nanofluid flow is assumed to be laminar and simulated within Re of 5–100. Hot-wall temperatures are $T_h = 310K$. The thermophysical properties of nanofluid are reported in Table 1.

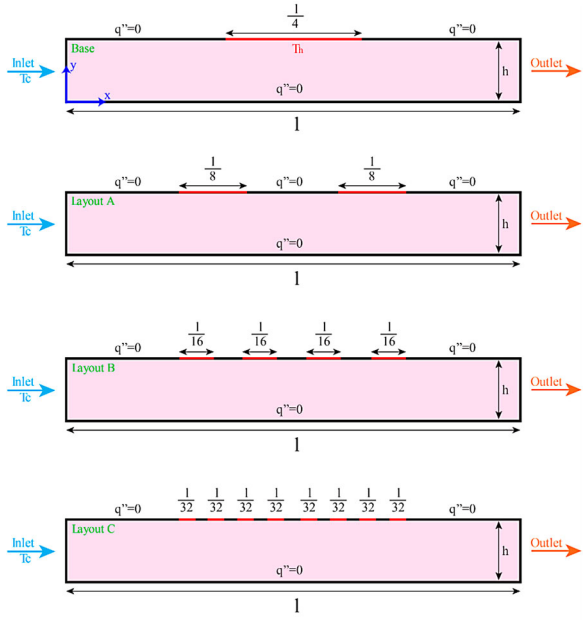

Figure 1. Different layout.

Table 1. Thermophysical properties of Al_2O_3-water (Jalali & Karimipour, 2019).

ϕ (%)	$\rho_{nf}(kgm^{-3})$	$\mu_{nf}(Pa.s)$	$k_{nf}(Wm^{-1}.K^{-1})$	$C_p(j\,kg^{-1}.K^{-1})$
0	997.1	$8.91*10^{-4}$	0.613	4179
2	1056.6	$9.37*10^{-4}$	0.6691	3922

3. Governing equations

In many studies, researchers have used numerical methods to describe physical phenomena (Dinarvand et al., 2021; Huang et al., 2022; Mahdavi et al., 2021; Moradi et al., 2020; Razavi et al., 2019; Wang et al., 2021). In this paper, single-phase model is used for the nanofluid. The basic non-dimension equations for continuity, momentum and energy equation, in stationary and incompressible flow, can be written as follows(Dinarvand et al., 2021; Mahdavi et al., 2021; Razavi et al., 2019; Tayebi et al., 2021):

$$\frac{\partial U}{\partial X}+\frac{\partial V}{\partial Y}=0 \tag{1}$$

$$U\frac{\partial U}{\partial X}+V\frac{\partial U}{\partial Y}=-\frac{\partial P}{\partial X}+\frac{\vartheta_{nf}}{\vartheta_f Re}\left(\frac{\partial^2 U}{\partial X^2}+\frac{\partial^2 U}{\partial Y^2}\right) \tag{2}$$

$$U\frac{\partial V}{\partial X}+V\frac{\partial V}{\partial Y}=-\frac{\partial P}{\partial Y}+\frac{\vartheta_{nf}}{\vartheta_f Re}\left(\frac{\partial^2 V}{\partial X^2}+\frac{\partial^2 V}{\partial Y^2}\right) \tag{3}$$

$$U\frac{\partial \theta}{\partial X}+V\frac{\partial \theta}{\partial Y}=\frac{\alpha_{nf}}{\alpha_f Re.Pr}\left(\frac{\partial^2 \theta}{\partial X^2}+\frac{\partial^2 \theta}{\partial Y^2}\right) \tag{4}$$

The dimensionless slip velocity is (Veera Krishna & Chamkha, 2021):

$$U_s=\pm\beta^*\left(\frac{\partial U}{\partial Y}\right)_{Y=0,1} \tag{5}$$

where β^* is dimensionless slip coefficient. Also, the dimensionless parameters involved in Equations (1–4) are:

$$\begin{aligned} &X=\frac{x}{h},\quad Y=\frac{y}{h},\quad U=\frac{u}{u_c},\quad V=\frac{v}{u_c},\\ &H=\frac{h}{h},\quad L=\frac{l}{h},\quad \beta^*=\frac{\beta}{h}\\ &\theta=\frac{T-T_c}{T_h-T_c},\quad P=\frac{\bar{p}}{\rho_{nf}{u_c}^2},\\ &Re=\frac{u_c h}{\vartheta_{nf}},\quad Pr=\frac{\vartheta_{nf}}{\alpha_{nf}}, \end{aligned} \tag{6}$$

Boundary conditions:

$$\begin{aligned} &U=1,V=0,\theta=0 && (X=0,0\le Y\le 1)\\ &V=0,\frac{\partial U}{\partial X} && \left(Y=\frac{l}{h},0\le Y\le 1\right)\\ &U=-U_s,\frac{\partial \theta}{\partial Y}=0 && \left(0\le X\le\frac{l}{h},Y=0\right)\\ &U=U_s,\theta=1 && \left(0\le X\le\frac{l}{h},Y=1\right) \end{aligned} \tag{7}$$

The local and average Nusselt numbers are (Jalali & Karimipour, 2019):

$$Nu_x=-\frac{k_{nf}}{k_f}\left(\frac{\partial \theta}{\partial Y}\right)_{Y=0,1} \tag{8}$$

$$Nu_m=\frac{1}{L}\int_0^L Nu_x dX \tag{9}$$

Entropy generation shows the value of irreversibility that is usually attributed to heat transfer and friction. Generally, in this study, the local entropy generation includes frictional and thermal that obtained as follows (Esfahani et al., 2017; Kefayati, 2015):

$$\begin{aligned} &\dot{S}_f'''=\frac{\mu_{nf}}{T}\left[2\left[\left(\frac{\partial u}{\partial x}\right)^2+\left(\frac{\partial v}{\partial y}\right)^2\right]+\left(\frac{\partial u}{\partial y}+\frac{\partial v}{\partial x}\right)^2\right],\\ &\dot{S}_f=\iiint \dot{S}_f'''dV \end{aligned} \tag{10}$$

$$\begin{aligned} &\dot{S}_t'''=\frac{k_{nf}}{T^2}\left[\left[\left(\frac{\partial T}{\partial x}\right)^2+\left(\frac{\partial T}{\partial y}\right)^2\right]\right],\\ &\dot{S}_t=\iiint \dot{S}_t'''dV \end{aligned} \tag{11}$$

and the dimensionless form of local entropy generations:

$$\dot{N}_t = \frac{\dot{S}_t''' h^2}{k_f} \tag{12}$$

$$\dot{N}_f = \frac{\dot{S}_f''' h^2}{k_f} \tag{13}$$

The normalized dimensionless entropy generations rate per unit depth are:

$$N_t = \int \dot{N}_t dV \tag{14}$$

$$N_f = \int \dot{N}_f dV \tag{15}$$

It is worth mentioning that to obtain nanofluid properties, the following equations are used. To solve the density, the specific heat capacity viscosity, and effective thermal conductivity(Brinkman, 1952; Jalali & Karimipour, 2019; Patel et al., 2006):

$$\rho_{nf} = (1-\phi)\rho_f + \phi\rho_s \tag{16}$$

$$\alpha_{nf} = \frac{k_{eff}}{(\rho c_p)_{nf}} \tag{17}$$

$$(\rho c_p)_{nf} = (1-\phi)(\rho c_p)_f + \phi(\rho c_p)_s \tag{18}$$

$$\mu_{nf} = \frac{\mu_f}{(1-\phi)^{0.25}} \tag{19}$$

$$\frac{k_{eff}}{k_f} = \left(1 + \frac{k_s A_s}{k_f A_f} + c k_s P_e \frac{A_s}{k_f A_s}\right) \tag{20}$$

In Equation (20), c is an experimental constant and its value is 15000. K_f and K_s are the thermal conductivity of fluid and nanoparticles that are 0.613 and 40 W/mK, respectively.

The molecular area's ratio of the base-liquid and that of solid nanoparticles is as follows where P_e, $\frac{A_s}{A_f}$ and j are defined as follows:

$$\frac{A_s}{A_f} = \left(\frac{d_f}{d_s} + \frac{\phi}{1-\phi}\right) \tag{21}$$

P_e is a constant parameter and describes as follows:

$$P_e = \frac{j d_s}{\alpha_f} \tag{22}$$

In Equation (22), j is associated with the impact of the Brownian motion and is obtained as follows: where $Kb = 1.3807 \times 10^{-23}$ J/K (the Boltzmann constant) and the molecular diameter of water and solid nanoparticles is $d_f = 2$ A° and ds = 40 nm, respectively

$$j = \frac{2K_b T}{\pi \mu_f d_s^2} \tag{23}$$

4. Grid study and validation

The finite volume method (FVM) with second-order discretization (to have more accurate) is utilized for continuity, momentum, and energy equations. In addition, coupling of the pressure and velocity is implemented by the SIMPLE algorithm. Grid study is performed using four networks with different grid numbers (Table 2). The mean Nusselt number was used to examine the grid study. According to Table 2, for Network A, with the grid number of 7000, Nu_{ave} is 1.63. By doubling the number of meshes (Network B), Nu_{ave} is increased by 17.79%. This figure for networks of C and D is 3.12% and 1%. Since the difference between the results of C and D networks is acceptable, hence network C is selected and utilized.

For validation, the results of Raisi et al. (2011). In their study, the nanofluid flow in a microchannel with a constant temperature boundary was investigated by considering the slip condition. The comparison between the present study and Raisi et al. (2011) is shown in Figures 2 and 3. In Figure 2, local Nusselt number is depicted along the microchannel walls and in Figure 3 dimensionless slip velocity (as a function of vertical direction) at the microchannel outlet. As can be seen, the results are in good agreement with those of Raisi et al. (2011). Therefore, the methods of solving the conservation equations are reliable.

Table 2. Grid study.

Model	Grid number	Nu_{ave}	Error (%)
A	7000	1.63	–
B	14000	1.92	17.79
C	28000	1.98	3.12
D	56000	2	1

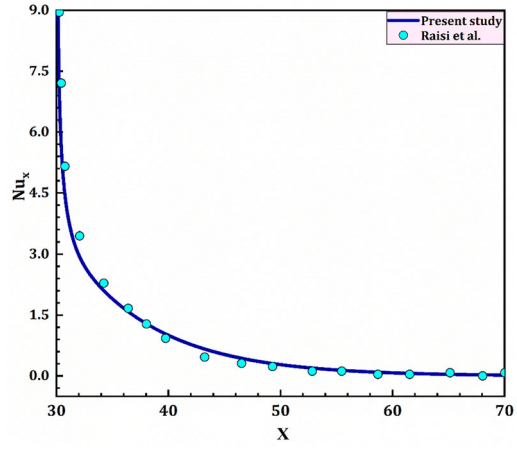

Figure 2. Comparative illustration of the Local Nusselt variations in the two studies.

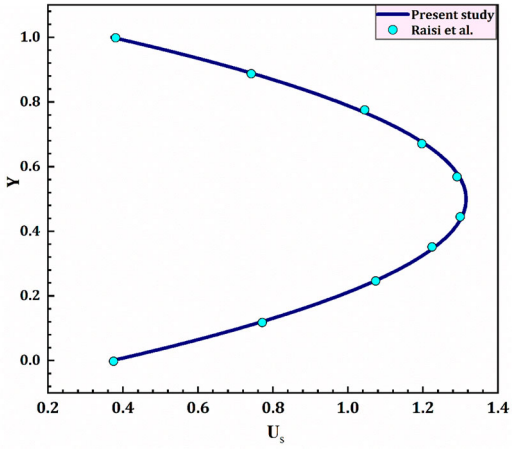

Figure 3. Comparative illustration of the dimensionless slip velocity profiles in the two studies.

5. Results

In the base microchannel, the constant temperature location on the wall remains constant. Whereas in other microchannels, constant temperature locations become smaller and smaller. It should be noted that in all microchannels, half of the upper wall is subjected to a constant temperature boundary condition ($T_H = 310K$). The other half of the wall is adiabatic. First, heat transfer through these microchannels investigate and then the thermal, viscose and $\dot{S}_{gen}$ will analyze considering the slip condition and non-slip condition.

5.1. Nusselt number

Figure 4 shows Nu_x along the upper microchannel wall in four different layouts. Simulations were performed at $\beta^* = 0.05$, and 0.02 vol.%. as well as Re of 5, 20, 60 and 100. In all microchannels, the highest Nu_x occurs at the entrance of the zones which is subjected to constant temperature boundary conditions and then, gradually decreases along the microchannel. In insulated zones where the temperature gradient is zero, Nu_x is also zero. For layout b, the two discontinuity created in the local Nusselt diagram corresponds to the two zones with a constant temperature boundary condition. The constant temperature locations are well illustrated in Figure 1. In other layouts, there is discontinuity caused by the presence of high-temperature locations.

If the calculation of $Nu_m = \frac{1}{L}\int_0^L Nu_x dX$ is performed, the mean value of Nu is obtained. The area under the curve for layout A is larger than that of the base case. This means that Nu_m for layout A is higher which is

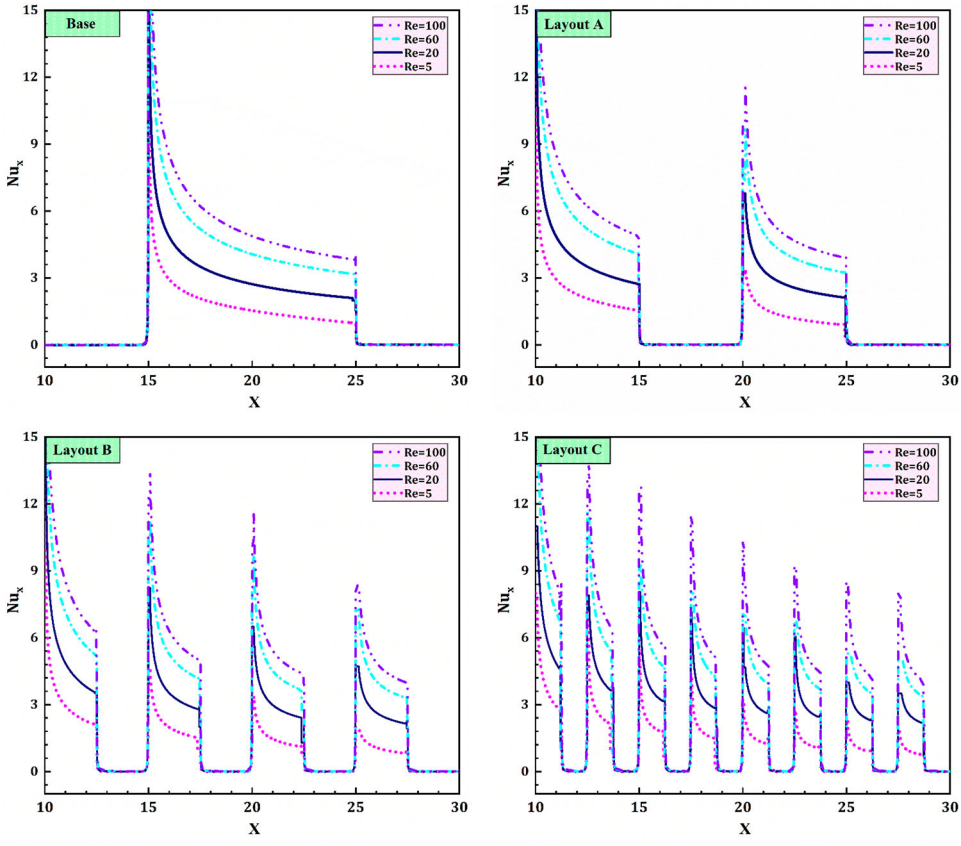

Figure 4. The effects of the presence of the zones with a constant temperature on Nu_x in various Re.

equivalent to more heat transfer in layout A than that of the base one.

From a physical point of view, in layout A, after the fluid passes through the first hot zone, the temperature of the fluid in the area close to the wall, increases. For the adiabatic zone, no extra thermal energy is added to the fluid molecules. Therefore, hot molecules have the opportunity to transfer energy to colder molecules through molecular collisions along with molecular diffusion. Therefore, in the adiabatic zones, the temperature distribution becomes more uniform and therefore the molecules near the upper wall become cooled. As the fluid approaches the second hot zone, these cold molecules can receive more heat from the hot wall because they have cooled in the previous zone (which was adiabatic). Therefore, as the number of hot zones increases, more heat is expected to transfer between the wall and the fluid.

Figure 5 shows Nu_{ave} for four layouts at $\beta^* = 0.05$, and 0.02 vol.%. As the *Re* rises, the temperature gradient decreases and hence HT improves. On the other hand, since Nu_{ave} is better for layout C, it can be concluded that applying a discontinuous-constant temperature boundary condition is better than the continuous one. The more the number of intermittent boundary conditions, the greater the impact on HT.

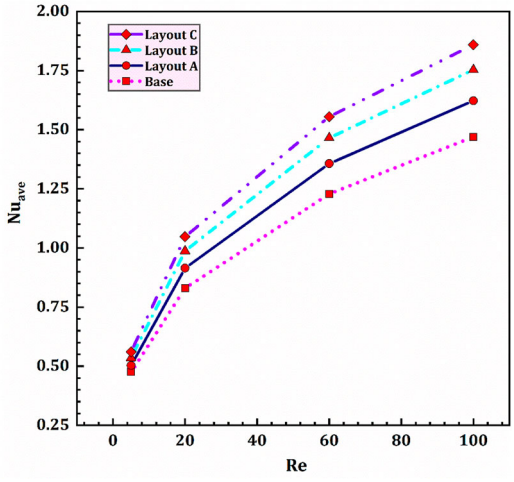

Figure 5. Efficacy of *Re* at each layout at 0.02 vol.% and $\beta^* = 0.05$.

Figure 6 shows Nu_{ave} of different layouts relative to the base microchannel. In this case, the base microchannel has a continuous-constant temperature boundary condition at $\beta^* = 0$.

Based on the results, at $\beta^* = 0$, Nu_{ave} of layouts of A, B and C is improved by 10, 19 and 26% compared to the base microchannel. Therefore, applying a discontinuous boundary condition can improve HT up to 26%. This figure at $\beta^* = 0.1$ is 53%. The heat transfer in the microchannel with slip condition is higher than the non-slip microchannel. Because applying the slip condition reduces the temperature gradient along the wall and hence enhances HT.

The temperature distribution for the four layouts is shown in Figure 7. It is observed that at higher the Reynolds (b), a smaller percentage of the fluid molecules have undergone a temperature gradient, or, at higher Reynolds (state B), the temperature variations in the fluid are concentrated in the vicinity of the wall.

5.2. Entropy generation

In this section, the effects of *Re*, β^* and the most important parameter of this study, namely applying discontinues-boundary conditions. As noted, $\dot{S}_{gen}$ is caused by the velocity and temperature gradients. The velocity gradient is responsible for $\dot{S}_f$ while the temperature gradient leads to the thermal entropy generation. First, $\dot{S}_f$ is examined. Figure 8 shows $\dot{S}_f$ for the four layouts. According to the results, $\dot{S}_f$ increases with increasing *Re*. Any rise in *Re* results in an increase in the velocity gradient in the microchannel which consequently raises the viscous entropy generation. More focus on Figure 8 reveals that the using discontinuous-boundary condition

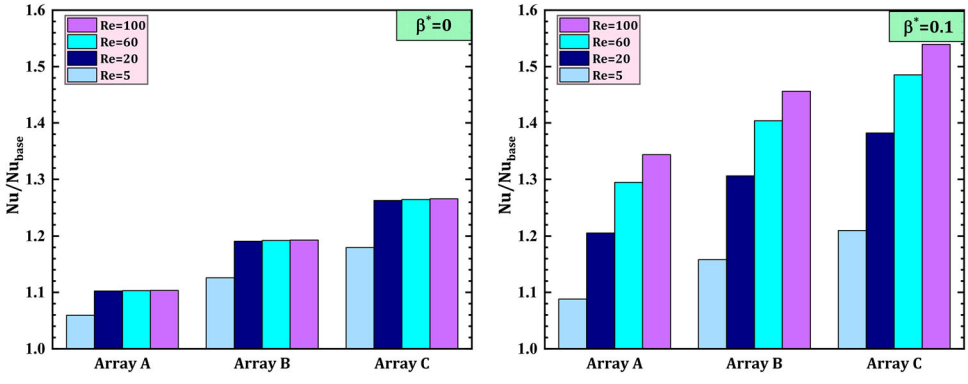

Figure 6. Average Nusselt number in each layout with respect to the base microchannel.

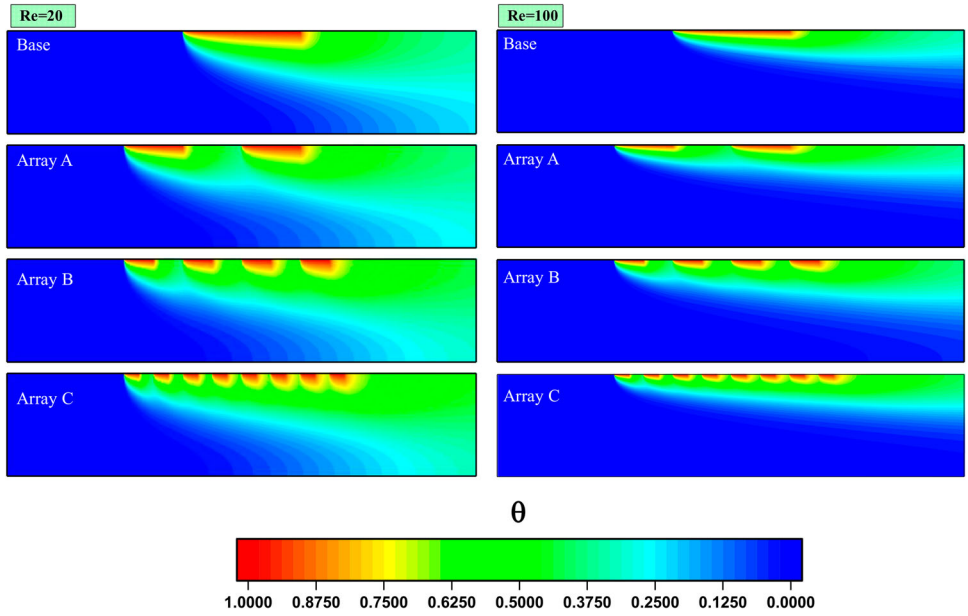

Figure 7. Temperature distribution in different layouts at Re = 20 and Re = 100.

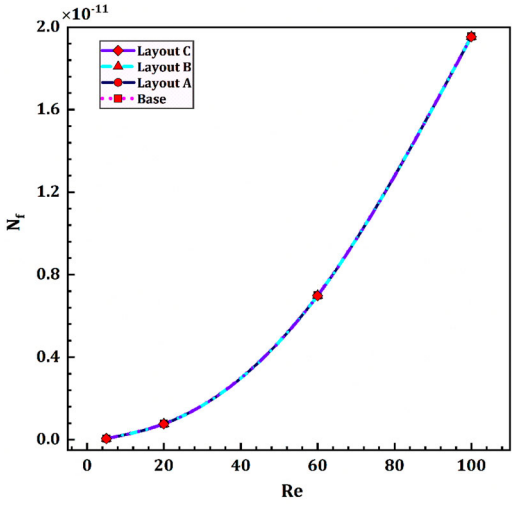

Figure 8. Effects of applying discontinuous-boundary condition on the viscous entropy generation.

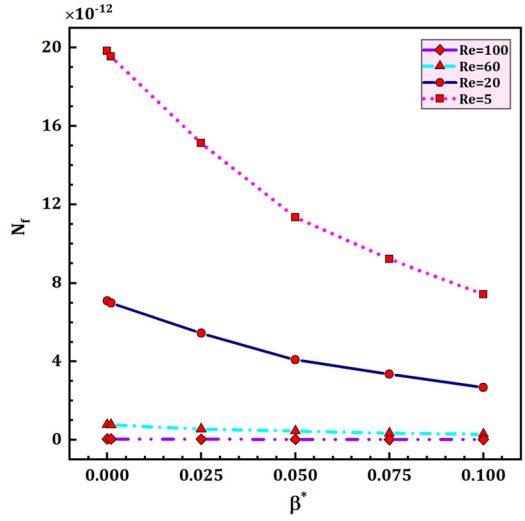

Figure 9. Effect of β^* on N_f (base layout).

(i.e. layouts of A, B and C) has no considerable effect on viscous entropy generation. Because $\dot{S}_f$ depends only on the velocity gradient. Changing the layout has no particular effect on the velocity gradient. As shown in Figure 8, applying discontinuous-boundary conditions only affects the temperature gradient.

Figure 9 shows $\dot{S}_f$ in terms of β^*. According to this figure, it can be seen that at $\beta^* = 0$ (microchannel with the non-slip condition) $\dot{S}_f$ is the highest. As β^* rises, the viscous entropy diminished. Because as β^* rises, the velocity gradient diminishes. Decreasing the velocity gradient results in a reduction in the viscosity-generation entropy term.

Figure 10 shows the effect of the layouts on the thermal entropy generation. As shown in Figure 10, it is observed that the effect of applying discontinuous-boundary conditions at the higher *Re* is more noticeable. As *Re* rises, the thermal boundary layer growth decreases. As the effect of applying discontinuous-boundary condition is more pronounced at higher *Re*, it is therefore predicted that at higher *Re*, the difference between the layouts of A, B and C are more.

It can be seen in Figure 10 that

- With increasing *Re*, $\dot{S}_t$ amplify owing to the growth in the temperature gradients

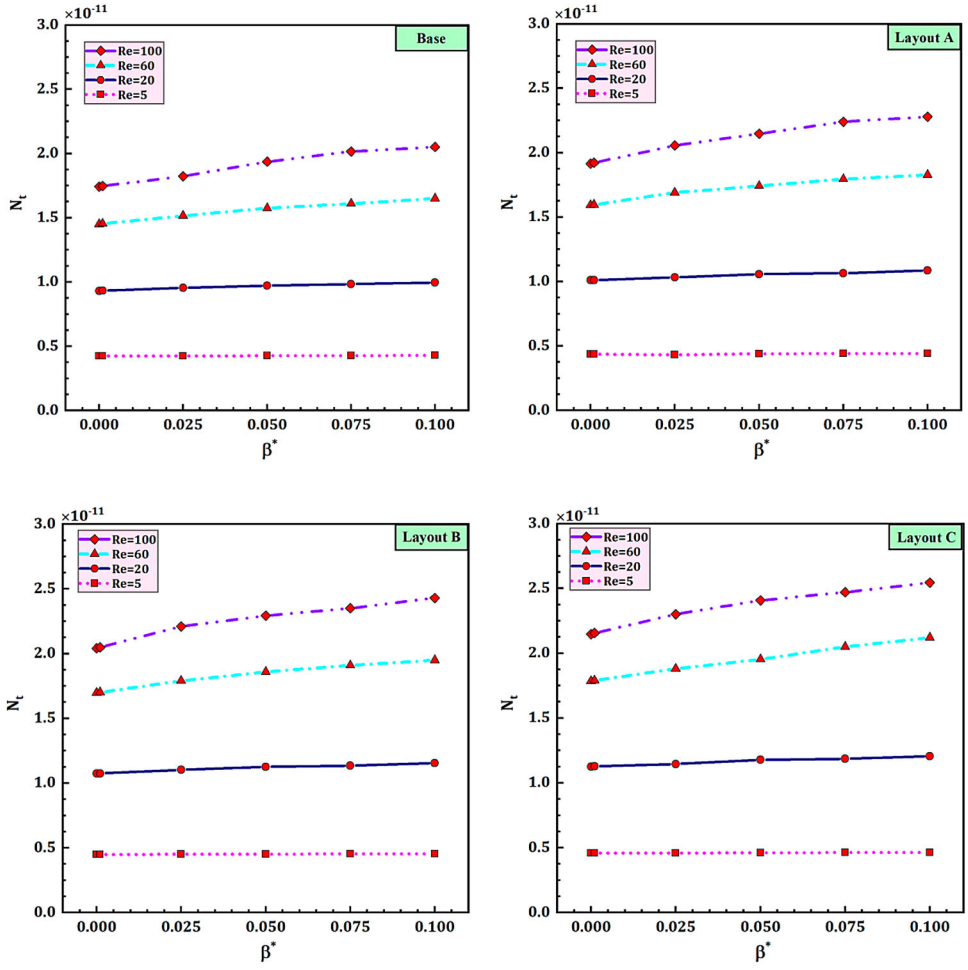

Figure 10. N_t at different layouts.

- Any growth in β^* improves HT (Figure 6). Higher HT means a higher temperature gradient, which subsequently intensifies the thermal entropy generation.
- Applying discontinuous-boundary conditions leads to HT improvement (Figure 6). The more HT is due to the higher temperature gradient. On the other hand, a higher temperature gradient means a higher rate of thermal entropy generation.

Figure 5 showed that the heat transfer for layouts A, B and C was higher than for the base case. Because the presence of adiabatic leads to the opportunity for warm molecules near the wall to transfer their energy to colder molecules. Therefore, the temperature in the adiabatic zone becomes uniform. This means that the temperature of the molecules close to the wall decreases. Thus, molecules close to the wall enter the next hot zones at lower temperatures. As the temperature difference in these areas increases, heat transfer intensifies. Although from the first law viewpoint, increasing the temperature difference is desirable (because it increases the heat transfer), but from the point of view of the second law, increasing the temperature difference is not very desirable. In other words, although the greater the temperature difference, the higher the heat transfer, but it should be noted that this heat transfer is accomplished with more irreversibility, which is not very desirable from the second law viewpoint. Therefore, in layouts A, B and C, heat transfer and entropy generation are higher than the base microchannel. Based on Figure 10, the microchannel with the continuous-boundary condition, if β^* is increased from 0 to 0.1, $\dot{S}_t$ will increase up to 13%. The same is true in the layouts of A, B and C. Increasing β^* from 0 to 0.1 leads to an increase in $\dot{S}_t$ up to 31% (for layout A), 39% (for layout B) and 46% (for layout C).

The distribution of $\dot{S}_t$ for each layout is shown in Figure 11. In the regions where the constant temperature boundary condition is applied, the concentration of $\dot{S}_t$ (zones marked in red) is high. Because in these zones, the temperature gradient is higher than in the other regions. On the other hand, at constant *Re* (e.g. 200), it is observed that in the layout of C, where the most discontinuity in the boundary condition is present, there is a greater thermal entropy generation. Therefore, the arrangement of

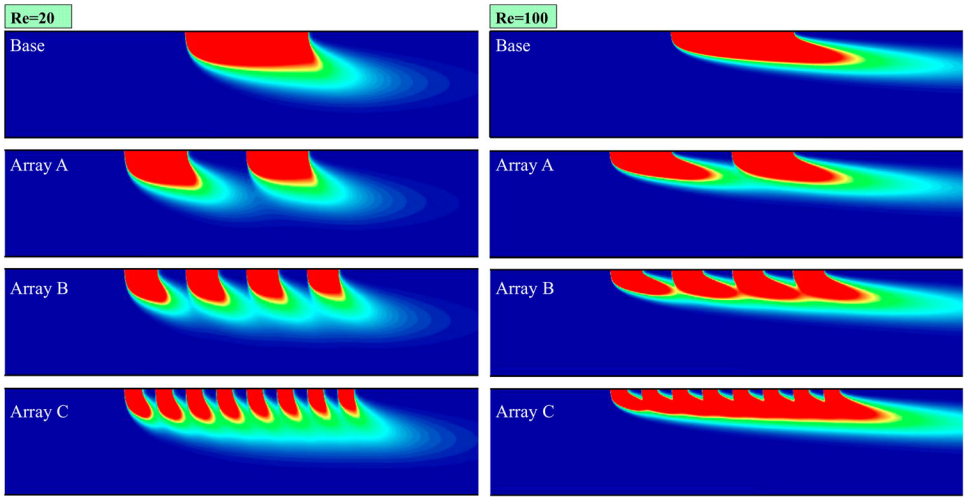

Figure 11. Thermal entropy generation at Re = 20 and Re = 100.

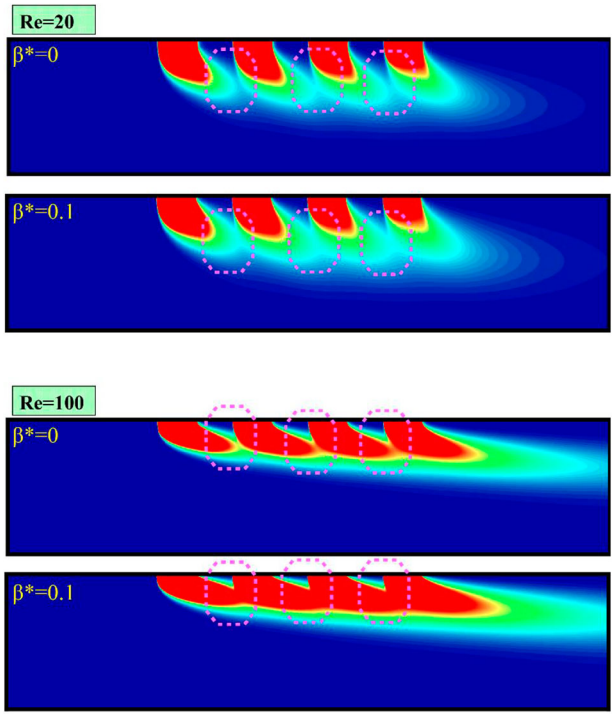

Figure 12. The effects of β^* on the thermal entropy generation at Re = 20 and Re = 100 (layout B).

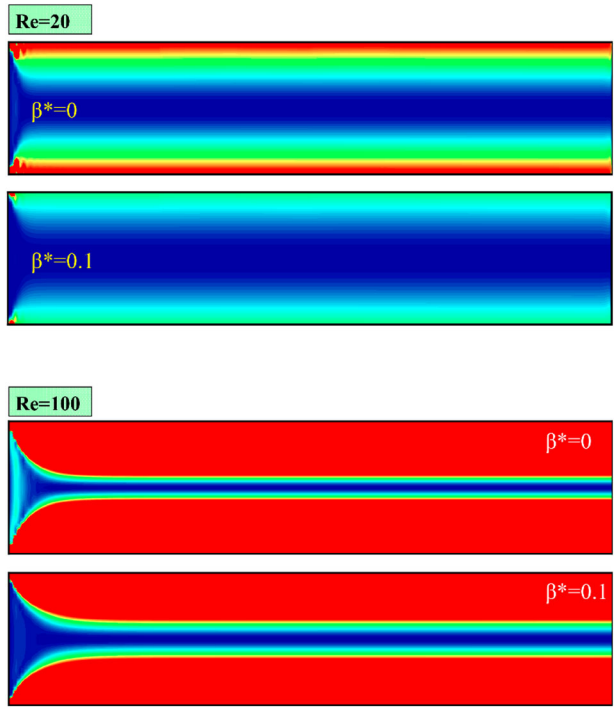

Figure 13. The effects of β^* on N_f at Re = 20 and Re = 100 (layout B).

using discontinuity-boundary conditions can affect the thermal entropy generation.

Figure 12 compares the distribution of $\dot{S}_t$ at $\beta^* = 0$ and $\beta^* = 0.1$. Note that the comparison is performed for layout B. In both Reynolds numbers, applying the slip condition causes the increase in a temperature gradient, hence $\dot{S}_t$ intensified. However, the effect of slip condition at higher *Re* is more pronounced. On the other hand, the effect of β^* on $\dot{S}_f$ is illustrated in Figure 13. The results prove that there is the highest distribution of $\dot{S}_f$ along the microchannel walls, and as the *Re* increases, $\dot{S}_f$ increases. Also, as β^* increases, the distribution of $\dot{S}_f$ in the microchannel center decreases.

6. Conclusion

In the current research four types of the microchannel with continuous-boundary conditions with equal heat sources' area were examined using the finite volume method. Moreover, the microchannels were analyzed by the impacts of various parameters such as Re number,

slip velocity on heat transfer, and entropy generation. The numerical results confirmed that the continuous-boundary conditions are highly beneficial to increasing the heat transfer which in comparison to the base microchannel HT boosted by 26%. Applying the slip condition changed the sensitivity of HT to the arrangement. At $\beta* = 0.1$, using discontinuous boundary conditions improved HT by 34, 45, and 53% for layouts A, B, and C, respectively. Based on the second law analysis main, It was found that applying discontinuous boundary conditions, did not affect the viscous entropy generation significantly although viscous entropy generation intensified with increasing Re while it reduced as $\beta*$ increased. As for thermal entropy generations, since continuous-boundary conditions played a vital role in increasing the temperature gradient, it increased the thermal entropy generation as a result of the higher gradient. Furthermore, if $\beta*$ increased from 0 to 0.1, $\dot{S}_t$ intensified up to 13%. This figure was 31% (for layout A), 39% (for layout B), and 46% (for layout C).

Nomenclature

A	Area (m^2)
c	experimental constant
C_p	Specific heat $\left(\frac{J}{kg.K}\right)$
d	Diameter (m)
h	Microchannel height (mm)
H	Dimensionless microchannel
HT	Heat transfer (W)
j	impact of the Brownian motion$\left(\frac{m}{s}\right)$
K_b	Boltzmann constant J/K
L	Dimensionless microchannel
$\dot{N}_f$	Dimensionless frictional entropy generation
$\dot{N}_t$	Dimensionless thermal entropy generation
Nu	Nusselt number
$\bar{p}$	Pressure (Pa)
P	Dimensionless pressure
P_e	constant parameter
Pr	Prandtl number
Re	Reynolds number
$\dot{S}_f$	Frictional entropy generation $\left(\frac{W}{K}\right)$
$\dot{S}'''_f$	Frictional entropy generation per volume$\left(\frac{W}{m^3.K}\right)$
$\dot{S}_{gen}$	Entropy generation $\left(\frac{W}{K}\right)$
$\dot{S}_t$	Thermal entropy generation $\left(\frac{W}{K}\right)$
$\dot{S}'''_t$	Thermal entropy generation per volume $\left(\frac{W}{m^3.K}\right)$
T	Temperature (K)
u	Horizontal velocity $\left(\frac{m}{s}\right)$
U	Dimensionless horizontal velocity
u_s	Slip velocity $\left(\frac{m}{s}\right)$
U_s	Dimensionless slip velocity
v	Vertical velocity $\left(\frac{m}{s}\right)$
V	Dimensionless vertical velocity
X, Y	Dimensionless horizontal/vertival coordinates

Greek letters

β^*	Dimensionless slip coefficient
β	Slip coefficient (mm)
φ	Volume fraction of nanoparticles (%)
μ	Dynamic viscosity $\left(\frac{N.s}{m^2}\right)$
θ	Dimensionless temperature
ρ	Density $\left(\frac{kg}{m^3}\right)$
ϑ	Kinematic viscosity $\left(\frac{m^2}{s}\right)$
α	Thermal diffusivity $\left(\frac{m^2}{s}\right)$

Super and subscripts

ave	average
c	cold
f	fluid
h	hot
nf	nanofluid
s	solid

Disclosure statement

No potential conflict of interest was reported by the author(s).

ORCID

Dariush Bahrami http://orcid.org/0000-0001-6676-4458
Kwok-Wing Chau http://orcid.org/0000-0001-6457-161X
Amir Mosavi http://orcid.org/0000-0003-4842-0613

References

Abo-Zahhad, E. M., Ookawara, S., Esmail, M. F. C., El-Shazly, A. H., Elkady, M. F., & Radwan, A. (2020). Thermal management of high concentrator solar cell using new designs of stepwise varying width microchannel cooling scheme. *Applied Thermal Engineering*, *172*, 115124. https://doi.org/10.1016/j.applthermaleng.2020.115124

Abo-Zahhad, E. M., Ookawara, S., Radwan, A., El-Shazly, A. H., & Elkady, M. F. (2019). Numerical analyses of hybrid jet impingement/microchannel cooling device for thermal management of high concentrator triple-junction solar cell. *Applied Energy*, *253*, 113538. https://doi.org/10.1016/j.apenergy.2019.113538

Ahmed, M., & Radwan, A. (2017). Performance evaluation of new modified low-concentrator polycrystalline silicon photovoltaic/thermal systems. *Energy Conversion and Management*, *149*, 593–607. https://doi.org/10.1016/j.enconman.2017.07.057

Al-Rashed, A. A. A. A., Shahsavar, A., Entezari, S., Moghimi, M. A., Adio, S. A., & Nguyen, T. K. (2019). Numerical investigation of non-Newtonian water-CMC/CuO nanofluid flow

in an offset strip-fin microchannel heat sink: Thermal performance and thermodynamic considerations. *Applied Thermal Engineering*, *155*, 247–258. https://doi.org/10.1016/j.applthermaleng.2019.04.009

Bahrami, A., Poshtiri, A. H., & Akbarpoor, A. M. (2019). Nusselt number correlations for forced convection in a microchannel including discrete heat sources. *Journal of Thermophysics and Heat Transfer*, *7*(11), 1–12. https://doi.org/10.2514/1.T5814

Brinkman, H. C. (1952). The viscosity of concentrated suspensions and solutions. *The Journal of Chemical Physics*, *20*(4), 571–571. https://doi.org/10.1063/1.1700493

Chamkha, A. J., Rashad, A. M., Mansour, M. A., Armaghani, T., & Ghalambaz, M. (2017). Effects of heat sink and source and entropy generation on MHD mixed convection of a Cu-water nanofluid in a lid-driven square porous enclosure with partial slip. *Physics of Fluids*, *29*(5), 052001. https://doi.org/10.1063/1.4981911

Dinarvand, M., Abolhasani, M., Hormozi, F., & Bahrami, Z. (2021). Cooling capacity of magnetic nanofluid in presence of magnetic field based on first and second laws of thermodynamics analysis. *Energy Sources, Part A: Recovery, Utilization, and Environmental Effects*, 1–17. https://doi.org/10.1080/15567036.2021.1872746

Ebrahimi, A., Rikhtegar, F., Sabaghan, A., & Roohi, E. (2016). Heat transfer and entropy generation in a microchannel with longitudinal vortex generators using nanofluids. *Energy*, *101*, 190–201. https://doi.org/10.1016/j.energy.2016.01.102

Esfahani, J., Akbarzadeh, M., Rashidi, S., Rosen, M., & Ellahi, R. (2017). Influences of wavy wall and nanoparticles on entropy generation over heat exchanger plat. *International Journal of Heat and Mass Transfer*, *109*, 1162–1171. https://doi.org/10.1016/j.ijheatmasstransfer.2017.03.006

Heshmatian, S., & Bahiraei, M. (2017). Numerical investigation of entropy generation to predict irreversibilities in nanofluid flow within a microchannel: Effects of Brownian diffusion, shear rate and viscosity gradient. *Chemical Engineering Science*, *172*, 52–65. https://doi.org/10.1016/j.ces.2017.06.024

Huang, K., Su, B., Li, T., Ke, H., Lin, M., & Wang, Q. (2022). Numerical simulation of the mixing behaviour of hot and cold fluids in the rectangular T-junction with/without an impeller. *Applied Thermal Engineering*, *204*, 117942. https://doi.org/10.1016/j.applthermaleng.2021.117942

Huminic, G., & Huminic, A. (2020). Entropy generation of nanofluid and hybrid nanofluid flow in thermal systems: A review. *Journal of Molecular Liquids*, *302*, 112533. https://doi.org/10.1016/j.molliq.2020.112533

Ishak, M. S., Alsabery, A. I., Chamkha, A., & Hashim, I. (2019). Effect of finite wall thickness on entropy generation and natural convection in a nanofluid-filled partially heated square cavity. *International Journal of Numerical Methods for Heat & Fluid Flow*, *22*(9), 122–139. https://doi.org/10.1108/HFF-06-2019-0505

Jalali, E., & Karimipour, A. (2019). Simulation the effects of cross-flow injection on the slip velocity and temperature domain of a nanofluid flow inside a microchannel. *International Journal of Numerical Methods for Heat & Fluid Flow*, *29*(5), 1546–1562. https://doi.org/10.1108/HFF-04-2018-0149

Jarray, A., Mehrez, Z., & El Cafsi, A. (2020). Effect of magnetic field on the mixed convection $$Fe _ 3O _ 4/water $$ Fe 3 O 4/water ferrofluid flow in a horizontal porous channel. *Pramana*, *94*(1), 1–12. https://doi.org/10.1007/s12043-020-02015-7

Kefayati, G. R. (2015). FDLBM simulation of entropy generation due to natural convection in an enclosure filled with non-Newtonian nanofluid. *Powder Technology*, *273*, 176–190. https://doi.org/10.1016/j.powtec.2014.12.042

Kuskov, K. V., Abedi, M., Moskovskikh, D. O., Serhiienko, I., & Mukasyan, A. S. (2021). Comparison of conventional and flash spark plasma sintering of Cu–Cr pseudo-alloys: Kinetics, structure, properties. *Metals*, *11*(1), 141. https://doi.org/10.3390/met11010141

Lai, W.-F., & Wong, W.-T. (2021). Property-tuneable microgels fabricated by using flow-focusing microfluidic geometry for bioactive agent delivery. *Pharmaceutics*, *13*(6), 787. https://doi.org/10.3390/pharmaceutics13060787

Li, Y., Moradi, I., Kalantar, M., Babadi, E., Malekahmadi, O., & Mosavi, A. (2021). Synthesis of new dihybrid nanofluid of TiO2/MWCNT in water–ethylene glycol to improve mixture thermal performance: Preparation, characterization, and a novel correlation via ANN based on orthogonal distance regression algorithm. *Journal of Thermal Analysis and Calorimetry*, *144*(6), 2587–2603. https://doi.org/10.1007/s10973-020-10392-9

Ma, D. D., Xia, G. D., Zong, L. X., Jia, Y. T., Tang, Y. X., & Zhi, R. P. (2019a). Experimental investigation of flow boiling heat transfer performance in zigzag microchannel heat sink for electronic cooling devices. *International Journal of Thermal Sciences*, *145*, 106003. https://doi.org/10.1016/j.ijthermalsci.2019.106003

Ma, Y., Mohebbi, R., Rashidi, M., & Yang, Z. (2019b). MHD convective heat transfer of Ag-MgO/water hybrid nanofluid in a channel with active heaters and coolers. *International Journal of Heat and Mass Transfer*, *137*, 714–726. https://doi.org/10.1016/j.ijheatmasstransfer.2019.03.169

Mahdavi, M., Sharifpur, M., Aybar, H. S., Chamkha, A. J., & Meyer, J. P. (2021). Impact of micro-fins on a heated cylinder submerged in a nanofluid saturated medium. *International Journal of Heat and Mass Transfer*, *177*, 121551. https://doi.org/10.1016/j.ijheatmasstransfer.2021.121551

Mansour, M., Janiga, G., Nigam, K., Thévenin, D., & Zähringer, K. (2018). Numerical study of heat transfer and thermal homogenization in a helical reactor. *Chemical Engineering Science*, *177*, 369–379. https://doi.org/10.1016/j.ces.2017.11.031

Mansour, M. A., Armaghani, T., Chamkha, A. J., & Rashad, A. M. (2019). Entropy generation and nanofluid mixed convection in a C-shaped cavity with heat corner and inclined magnetic field. *The European Physical Journal Special Topics*, *228*(12), 2619–2645. https://doi.org/10.1140/epjst/e2019-900050-3

Mehrez, Z., Cafsi, A. E., Belghith, A., & Quéré, P. L. (2015a). Effect of heated wall position on heat transfer and entropy generation of Cu–water nanofluid flow in an open cavity. *Canadian Journal of Physics*, *93*(12), 1615–1629. https://doi.org/10.1139/cjp-2014-0388

Mehrez, Z., & El Cafsi, A. (2017). Thermodynamic analysis of $$Al_2O_3$$–water nanofluid flow in an open cavity under pulsating inlet condition. *International Journal of Applied and Computational Mathematics*, *3*(1), 489–510. https://doi.org/10.1007/s40819-017-0366-9

Mehrez, Z., & El Cafsi, A. (2021a). Forced convection Fe3O4/water nanofluid flow through a horizontal channel under the influence of a non-uniform magnetic field. *The European Physical Journal Plus*, *136*(4), 451. https://doi.org/10.1140/epjp/s13360-021-01410-2

Mehrez, Z., & El Cafsi, A. (2021b). Heat exchange enhancement of ferrofluid flow into rectangular channel in the presence of a magnetic field. *Applied Mathematics and Computation*, *391*, 125634. https://doi.org/10.1016/j.amc.2020.125634

Mehrez, Z., El Cafsi, A., Belghith, A., & Le Quéré, P. (2015b). MHD effects on heat transfer and entropy generation of nanofluid flow in an open cavity. *Journal of Magnetism and Magnetic Materials*, *374*, 214–224. https://doi.org/10.1016/j.jmmm.2014.08.010

Mohammadian, S. K., Reza Seyf, H., & Zhang, Y. (2014). Performance augmentation and optimization of aluminum oxide-water nanofluid flow in a two-fluid microchannel heat exchanger. *Journal of Heat Transfer*, *136*(2), 2. https://doi.org/10.1115/1.4025431

Moradi, I., Karimipour, A., Afrand, M., Li, Z., & Bach, Q.-V. (2020). Three-dimensional numerical simulation of external fluid flow and heat transfer of a heat exchanger in a wind tunnel using porous media model. *Journal of Thermal Analysis and Calorimetry*, *141*(5), 1647–1667. https://doi.org/10.1007/s10973-020-10184-1

Patel, H. E., Anoop, K., Sundararajan, T., & Das, S. K. (2006). *A micro-convection model for thermal conductivity of nanofluids*. Paper presented at the International heat transfer conference 13, London, UK, 12 May 2006.

Radwan, A., Ahmed, M., & Ookawara, S. (2016). Performance enhancement of concentrated photovoltaic systems using a microchannel heat sink with nanofluids. *Energy Conversion and Management*, *119*, 289–303. https://doi.org/10.1016/j.enconman.2016.04.045

Raisi, A., Ghasemi, B., & Aminossadati, S. (2011). A numerical study on the forced convection of laminar nanofluid in a microchannel with both slip and no-slip conditions. *Numerical Heat Transfer, Part A: Applications*, *59*(2), 114–129. https://doi.org/10.1080/10407782.2011.540964

Rashad, A. M., Armaghani, T., Chamkha, A. J., & Mansour, M. A. (2018). Entropy generation and MHD natural convection of a nanofluid in an inclined square porous cavity: Effects of a heat sink and source size and location. *Chinese Journal of Physics*, *56*(1), 193–211. https://doi.org/10.1016/j.cjph.2017.11.026

Rashad, A. M., Mansour, M. A., Armaghani, T., & Chamkha, A. J. (2019). MHD mixed convection and entropy generation of nanofluid in a lid-driven U-shaped cavity with internal heat and partial slip. *Physics of Fluids*, *31*(4), 042006. https://doi.org/10.1063/1.5079789

Razavi, S. E., Farhangmehr, V., & Babaie, Z. (2019). Numerical investigation of hemodynamic performance of a stent in the main branch of a coronary artery bifurcation. *BioImpacts: Bi*, *9*(2), 97–103. https://doi.org/10.15171/bi.2019.13

Shashikumar, N., Gireesha, B., Mahanthesh, B., Prasannakumara, B., & Chamkha, A. J. (2018). Entropy generation analysis of magneto-nanoliquids embedded with aluminium and titanium alloy nanoparticles in microchannel with partial slips and convective conditions. *International Journal of Numerical Methods for Heat & Fluid Flow*, *5*(9), 38–45. https://doi.org/10.1108/HFF-06-2018-0301

Singh, P. K., Anoop, K. B., Sundararajan, T., & Das, S. K. (2010). Entropy generation due to flow and heat transfer in nanofluids. *International Journal of Heat and Mass Transfer*, *53*(21), 4757–4767. https://doi.org/10.1016/j.ijheatmasstransfer.2010.06.016

Sun, L., Wang, G., Zhang, C., Jin, Q., & Song, Y. (2021). On the rheological properties of multi-walled carbon nano-polyvinylpyrrolidone/silicon-based shear thickening fluid. *Nanotechnology Reviews*, *10*(1), 1339–1348. https://doi.org/10.1515/ntrev-2021-0087

Tayebi, T., & Chamkha, A. J. (2019). Entropy generation analysis during MHD natural convection flow of hybrid nanofluid in a square cavity containing a corrugated conducting block. *International Journal of Numerical Methods for Heat & Fluid Flow*, *13*(8), 66–76. https://doi.org/10.1108/HFF-04-2019-0350

Tayebi, T., Dogonchi, A. S., Karimi, N., Ge-JiLe, H., Chamkha, A. J., & Elmasry, Y. (2021). Thermo-economic and entropy generation analyses of magnetic natural convective flow in a nanofluid-filled annular enclosure fitted with fins. *Sustainable Energy Technologies and Assessments*, *46*, 101274. https://doi.org/10.1016/j.seta.2021.101274

Tian, M.-W., Parikhani, T., Jermsittiparsert, K., & Ashraf, M. A. (2020). Exergoeconomic optimization of a new double-flash geothermal-based combined cooling and power (CCP) system at two different cooling temperatures assisted by boosters. *Journal of Cleaner Production*, *261*.(4), 69–88. https://doi.org/10.1016/j.jclepro.2020.120921.

Toghraie, D., Mashayekhi, R., Arasteh, H., Sheykhi, S., Niknejadi, M., & Chamkha, A. J. (2019). Two-phase investigation of water-Al2O3 nanofluid in a micro concentric annulus under non-uniform heat flux boundary conditions. *International Journal of Numerical Methods for Heat & Fluid Flow*, *9*(8), 117–133. https://doi.org/10.1108/HFF-11-2018-0628

Torosyan, K. S., Sedegov, A. S., Kuskov, K. V., Abedi, M., Arkhipov, D. I., Kiryukhantsev-Korneev, P. V., Vorotilo StepanMoskovskikh Dmitry O., Mukasyan, A. S. (2020). Reactive, nonreactive, and flash spark plasma sintering of Al2O3/SiC composites—A comparative study. *Journal of the American Ceramic Society*, *103*(1), 520–530. https://doi.org/10.1111/jace.16734

Vajdi, M., Moghanlou, F. S., Niari, E. R., Asl, M. S., & Shokouhimehr, M. (2020). Heat transfer and pressure drop in a ZrB2 microchannel heat sink: A numerical approach. *Ceramics International*, *46*(2), 1730–1735. https://doi.org/10.1016/j.ceramint.2019.09.146

Veera Krishna, M., & Chamkha, A. J. (2021). Thermo-diffusion, Chemical reaction, Hall and ion slip effects on MHD rotating flow of micro-polar fluid past an infinite vertical porous surface. *International Journal of Ambient Energy*, *7*(11), 1-29. https://doi.org/10.1080/01430750.2021.1946146

Wang, Y., Wang, H., Zhou, B., & Fu, H. (2021). Multi-dimensional prediction method based on Bi-LSTMC for ship roll. *Ocean Engineering*, *242*, 110106. https://doi.org/10.1016/j.oceaneng.2021.110106

Weiß, A., Popp, T., Zinn, G., Preißinger, M., & Brüggemann, D. (2019). A micro-turbine-generator-construction-kit (MTG-c-kit) for small-scale waste heat recovery ORC-plants. *Energy*, *181*, 51–55. https://doi.org/10.1016/j.energy.2019.05.135

Xu, H., He, T., Zhong, N., Zhao, B., & Liu, Z. (2022). Transient thermomechanical analysis of micro cylindrical asperity sliding contact of SnSbCu alloy. *Tribology International*, *167*, 107362. https://doi.org/10.1016/j.triboint.2021.107362

Yang, Y.-T., Wang, Y.-H., & Huang, B.-Y. (2015). Numerical optimization for nanofluid flow in microchannels using entropy generation minimization. *Numerical Heat Transfer, Part A: Applications*, *67*(5), 571–588. https://doi.org/10.1080/10407782.2014.937282

Zahmatkesh, I., Sheremet, M., Yang, L., Heris, S. Z., Sharifpur, M., Meyer, J. P., Ghalambaz MohammadWongwises SomchaiJing Dengwei, Mahian, O. (2021). Effect of nanoparticle shape on the performance of thermal systems utilizing nanofluids: A critical review. *Journal of Molecular Liquids*, *321*, 114430. https://doi.org/10.1016/j.molliq.2020.114430

Zamzari, F., Mehrez, Z., Cafsi, A. E., Belghith, A., & Quéré, P. L. (2015). Entropy generation and mixed convection in a horizontal channel with an open cavity. *International Journal of Exergy*, *17*(2), 219–239. https://doi.org/10.1504/IJEX.2015.069993